Int. J. Electrochem. Sci., 16 **(2021)** Article Number: 211214, doi: 10.20964/2021.12.14

International Journal of
ELECTROCHEMICAL
SCIENCE
www.electrochemsci.org

Short Communication

Experimental and theoretical studies of 2-cyano-N-(4-morpholinobenzyldine) acetohydrazide as corrosion inhibitor for galvanized steel and 304 stainless steel in 1M H_2SO_4 solution

Ghalia A. Gaber[1], *Shimaa Hosny*[2], *Lamiaa Z. Mohamed*[3,*]

[1] Department of Chemistry, Faculty of Science (Girls), Al-Azhar University, P.O. Box: 11754, Yousef Abbas Str., Nasr City, Cairo, Egypt
[2] Chemistry Department, Faculty of Science, New Valley University, El-Kharga, 72511, Egypt
[3] Mining, Petroleum and Metallurgical Engineering Department, Faculty of Engineering, Cairo University, Egypt
[*]E-mail: lamylomy@yahoo.com

Received: 20 August 2021 / *Accepted:* 22 September 2021 / *Published:* 10 November 2021

A 2-cyano-N-(4-morpholinobenzyldine) acetohydrazide is used as a corrosion inhibitor for both galvanized steel (GS) and 304 stainless steel (304 SS) in 1M H_2SO_4. The corrosion inhibition efficiency of GS and 304 SS in 1M H_2SO_4 were studied using both chemical (weight-loss (WL)) and electrochemical techniques. The obtained results were used for calculating the inhibition effectiveness, corrosion rate (CR), and adsorption characteristics. The inhibitors adhere to the Langmuir adsorption isotherm on the investigated different surfaces. The SEM micrographs were investigated of GS and 304 SS with and without inhibitors at optimum conditions. The inhibitor led to a smooth and dense protective layer formation. Quantum chemical investigation of 2-cyano-N-(4-morpholinobenzyldine) acetohydrazide was studied.

Keywords: Corrosion inhibitor; Galvanized steel; 304 stainless steel; Acidic solution; 2-cyano-N-(4-morpholinobenzyldine) acetohydrazide

1. INTRODUCTION

Corrosion changes the material properties with its surroundings, which impair material function and possibly the environment [1, 2]. Corrosion inhibition is a signification issue for studying and enhancement the corrosion behavior by increasing the corrosion resistance in all branches of technology [3, 4]. Its selection influencing by temperature, kind of metal, concentration and flow rate of the corrosive media, its purpose is to reduce the corrosion rate (CR) by lowering the anodic rate, cathodic rate, or both corrosion reactions. The different types of inhibitors are anodic, cathodic and mixed

inhibitors [5]. Mixed inhibitors are organic chemicals that control both metal dissolution and cathodic reaction, decelerating and controlling corrosion, used in chemical, petrochemical and oil exploration industries. The researchers needed to develop a new organic corrosion inhibitors with low cost, high availability and sufficient adsorption and good performance for the different environmental profiles. Heteroatoms (N, O, or S), multiple bonds, and/or aromatic rings should all be present in the inhibitor molecule, be soluble and stable in the used medium and green environmentally [6, 7]. The hydrazide derivatives have been deeply investigated their performance for corrosion inhibitive in acid media on mild steel [8]. The corrosion of several organic compounds were investigated in 1 M HCl on mild steel [9, 10]. Finding that as the concentration of all examined substances raised, it increases their inhibition performance. The researchers also looked into quantum chemistry to see whether they can link inhibitor molecular structures to inhibition effects [5, 10-11]. The inhibitors usage is one of the most cost-effective ways to protect mild steel surfaces against corrosion in the industry [16]. The majority of organic inhibitors are heterocyclic molecules such as azoles, pyridine and imidazoline [17-19], or like polymers [20, 21].

The aim of the work is to investigate the experimental and theoretical behavior of 2-cyano-N-(4-morpholinobenzyldine) acetohydrazide as a corrosion protection of galvanized steel (GS) and 304 stainless steel (SS) in 1M H_2SO_4 solution by the weight-loss (WL) method, electrochemical technique and surface morphology. Quantum chemical investigation of 2-cyano-N-(4-morpholinobenzyldine) acetohydrazide were studied.

2. EXPERIMENTAL WORK

2.1 Synthesis of the Schiff base Ligand CMBAH

Preparing pure ethanol (50 ml) with 1 ml glacial acetic acid and 0.3 g sodium acetate anhydrous, a mixture of 4-morpholinobenzaldehyde (1.91 g, 0.01 mol) and 2-cyanoacetohydrazide (0.99 g, 0.01 mol) was refluxed for 6 h. The product was cooled to room temperature (RT) before being filtered and recrystallized from ethanol, then dried under vacuum to provide yellow crystals with 83% yield, m.pt. 170 ° C. The proposed ligand formula ($C_{14}H_{16}N_4O_2$, F.W. = 272.30) well agree with the stoichiometry derived from analytical data and mass spectra, as existed in Scheme 1:

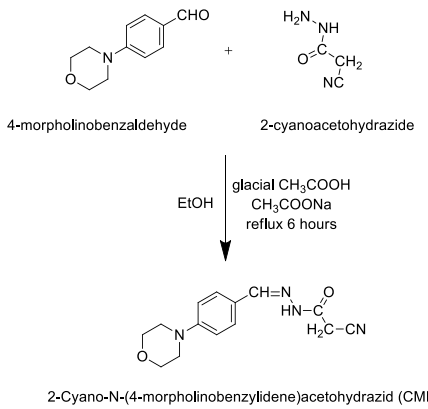

Scheme 1. Synthesis of the ligand CMBAH.

2.2 Materials

The galvanized steel has a 25 µm thickness of pure zinc. The chemical composition of 304 SS is 18%Cr, 8%Ni, 2%Mn, 0.03%S, 0.08%C, 0.75%Si, 0.045%P and balance is Fe.

2.3 Weight-loss Method (WL)

The corrosion is measured periodically for GS and 304 SS. The initial weight of the polished investigated samples were measured. The samples were suspended in duplicate into the solution using glass hooks and a 100 mL beaker for solutions. Prior to immersion in a 1M H_2SO_4 solution, the GS and 304 SS specimens were weighed. The specimens were released after 1, 2, 3, and 4 h, rinsed with water, dried, and weighed to four decimal accuracy. The WL is the difference between weight before and after immersion in the solution. The experiment was repeated for the inhibitor concentrations (0, 50, 100, 150 and 200 ppm) in 1M H_2SO_4. The CR in mm/y is calculated as follows Eq. 1 [12, 13]:

$$\mathrm{CR(mm/y)} = \frac{\mathrm{\Delta WxK}}{\mathrm{AxTxD}} \qquad (1)$$

where: K = a constant ($8.76x10^4$), T = time of exposure in h, A = area in cm^2, ΔW = weight-loss in grams, and D = density in g/cm^3.

The inhibition efficiency (IE) and surface coverage (θ) are determined by:

$$\mathrm{IE\ \%} = \frac{\mathrm{CRo - CRinh}}{\mathrm{CRo}}\ \mathrm{x}\ 100 \qquad (2)$$

Where CR_0 and CR_{inh} are the CR of specimens in the presence and absence of inhibitor, separately [14].

$$\mathrm{The\ level\ of\ surface\ coverage\ (\theta)} = \frac{\mathrm{IE}}{100} \qquad (3)$$

2.4. Potentiodynamic polarization estimations

Potentiodynamic polarization curves for GS and 304 SS in corrosive media were swept at a rate of 0.2 mV/s between – 1.0 and + 1.0 V. Prior to the corrosion experimental, the operating electrode was submerged in the test solution for 30 minutes to provide a quasi-stationary estimate of the open circuit potential. Values of current and potential of corrosion (I_{corr} and E_{corr}) were measured using the intersection of the linear cathodic and anodic branches of Tafel plots in the presence and absence of various concentrations of investigated inhibitor. The surface inclusion degrees (θ) and inhibitive efficiency (IE %) were also calculated in potentiodynamic measurements.

2.5 Surface Morphology

The corroded GS and 304 SS surface morphologies in absence and presence of 2-cyano-N-(4-morpholinobenzyldine) acetohydrazide as a corrosion inhibitor were investigated.

3. RESULTS AND DISCUSSION

3.1. Ligand CMBAH Characterization

The Schiff base Ligand CMBAH structure was investigated by elemental analyses, IR, UV-Vis, and mass spectra. Anal. calculated %: C, 61.75; H, 5.92; N, 20.58. Found%: C, 61.84; H, 5.93; N, 20.53. The IR spectrum (cm^{-1}) bands of the ligand at 3170, 1679, 1628, 1611, 1312 and 1090, corresponding to υ(NH), υ(C=O)amide, δ(NH), υ(C=N)azomethine, υ(C-N), and υ(C-O), respectively [15].

The electronic absorption spectrum, λ_{max}(nm), of the ligand (10^{-3} M in DMF), revealed three different bands at 290, 355 and 410 which can be attributed to π- π* transition inside the aromatic system, π- π* transition inside C=N and an intermolecular charge transfer (CT) transition within the entire molecule. The CMBAH mass spectrum illustrates the molecular ion peak at m/e = 272.33 amu, which confirms the formula weight (F.W. = 272.30) as provided in Fig. 1. The mass fragmentation pattern supported the suggested structure of the CMBAH as given in Scheme 2.

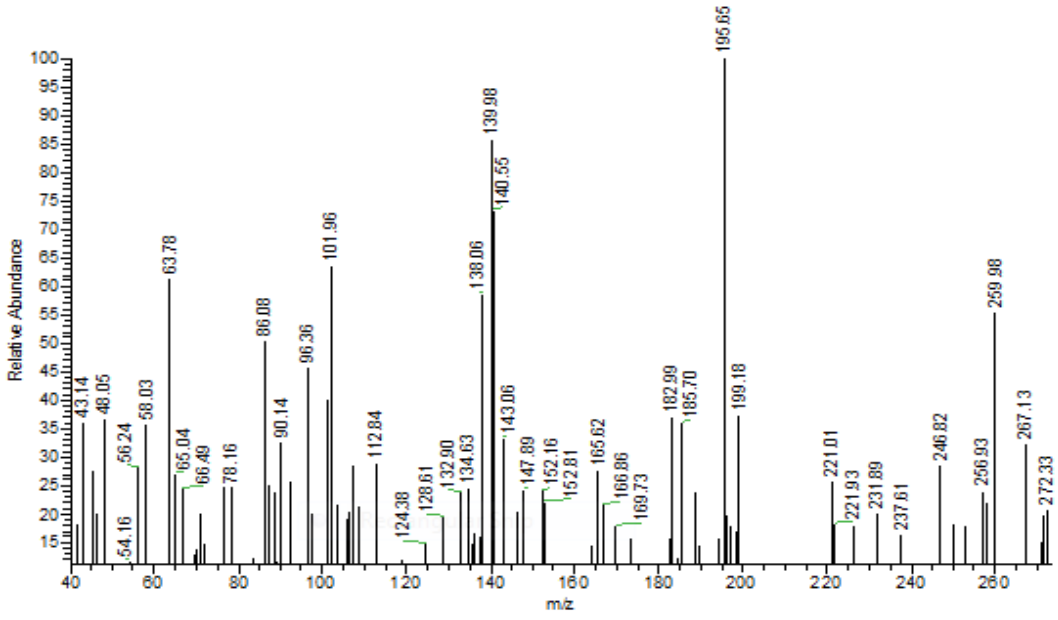

Figure 1. Mass spectrum of the ligand CMBAH

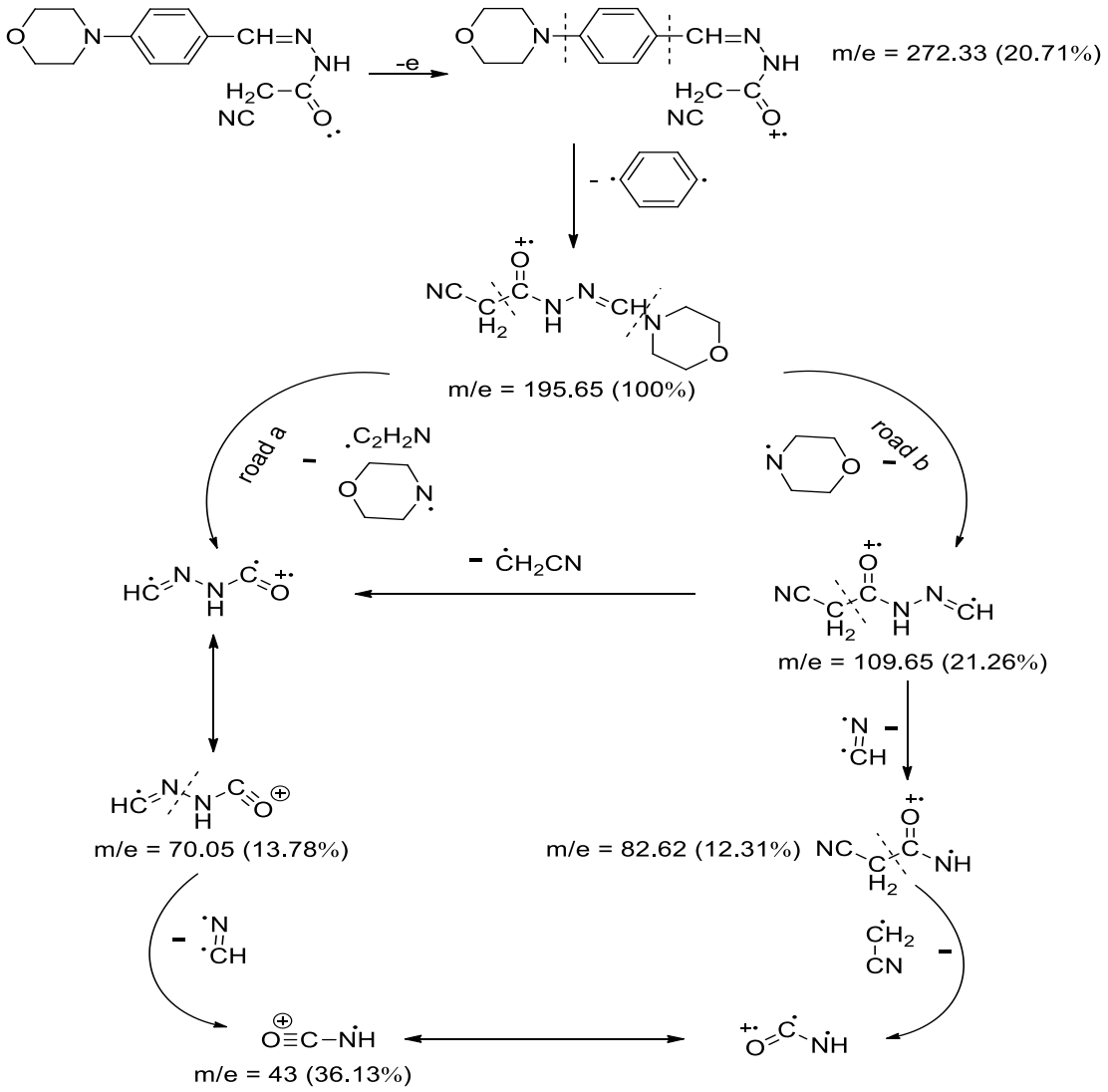

Scheme 2. Mechanism of mass fragmentation of Schiff base ligand

3.2 Weight-loss Method (WL)

3.2.1 Effect of inhibitor concentration

The corrosion rates of GS and 304 SS in 1M H_2SO_4 for various concentrations of 2-cyano-N-(4-morpholinobenzyldine) acetohydrazide inhibitor were determined after 4 h of immersion. At RT and concentrations of 2-cyano-N-(4-morpholinobenzyldine) acetohydrazide in 1M H_2SO_4 acid, the corrosion of GS and 304 SS were reduced. The percentage inhibition efficiency rate (IE %) and CR from WL method at various concentrations of investigated inhibitor are provided in Table 1 and provided in Table 1. The presence of a protective film on the electrode surface and the decrease in the effective electron transfer rate at the interface led to the maximum protection efficiency against corrosion of 304 SS at 50 ppm concentration was about 93 %. Table 1 demonstrates that WL and CR progressively decreased with inhibitor concentration. The best protection appears on 304 SS at 50 ppm investigated inhibitor but the zinc layer easily dissolution in GS.

Table 1. Inhibition efficiencies, CR, Degree of coverage of various concentrations of investigated inhibitor (0-200 ppm) for corroded GS and 304 SS in 1M H_2SO_4 after 4 h at RT.

Inhibitor concentrations in 1 M H_2SO_4 (ppm)	GS				304 SS			
	WL, g	CR, mm/y	θ	IE, %	WL, g	CR, mm/y	θ	IE, %
0	0.199	248.82	--	--	0.082	114.24	--	--
50	0.167	207.77	0.165	16.49	0.006	8.37	0.927	92.67
100	0.169	211.14	0.151	15.14	0.015	20.92	0.817	81.68
150	0.178	222.62	0.105	10.53	0.016	22.32	0.805	80.46
200	0.170	212.01	0.148	14.79	0.016	22.32	0.805	80.46

3.2.2 Adsorption isotherm

The surface coverage (θ) for investigated inhibitor concentrations was calculated. From Fig. 2, a plot of C/θ versus C gives a straight line which indicated that the investigated inhibitor obeyed Langmuir adsorption isotherm. Concluding that the maximum inhibition corresponds to the adsorbed layer formation of the inhibitor on the active sites of the metal surface GS and 304 SS.

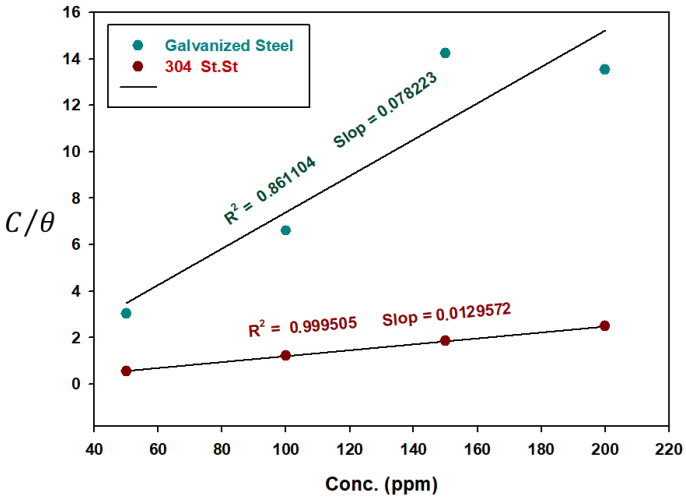

Figure 2. Langmuir's plot of inhibitors in 1M H_2SO_4.

3.2.3 Effect of immersion time

Tables 2 and 3 demonstrate the effect of immersion time on the corrosion of the GS and the 304 SS in 1M H_2SO_4 with different conditions. The CR obtained from WL of GS and 304 SS in 1M H_2SO_4 with different concentrations of 2-cyano-N-(4-morpholinobenzyldine) acetohydrazide at different

immersion time is tabulated in Tables 2 and 3. The CR significantly decreased as the immersion period was increased up to 4 h, where the protection efficiency increased. The protective film formation on the electrode surface of GS or 304 SS increases the protection efficiency values.

Table 2. The WL results of GS in 1M H_2SO_4 with (0-200 ppm) concentrations of investigated inhibitor at different immersion time.

Time, h	Concentration of inhibitor in 1M H_2SO_4, ppm									
	0		50		100		150		200	
	WL, g	CR, mm/y	WL, g	CR, mm/y	WL, g	CR, mm/y	WL, g	CR, mm/y	WL, g	CR, mm/y
1	0.163	811.11	0.139	691.32	0.152	758.70	0.153	763.69	0.154	766.19
2	0.171	426.77	0.154	383.09	0.156	388.09	0.170	424.27	0.156	388.09
3	0.174	289.50	0.157	260.89	0.164	272.53	0.173	287.34	0.160	266.54
4	0.199	248.82	0.167	207.77	0.169	211.14	0.178	222.62	0.170	212.01

Table 3. The WL results of 304 SS in 1M H_2SO_4 with (0-200 ppm) concentrations of investigated inhibitor at different immersion time.

Time, h	Concentration of inhibitor in 1M H_2SO_4, ppm									
	0		50		100		150		200	
	WL, g	CR, mm/y	WL, g	CR, mm/y	WL, g	CR, mm/y	WL, g	CR, mm/y	WL, g	CR, mm/y
1	0.085	473.71	0.005	27.89	0.002	11.16	0.007	36.27	0.014	75.32
2	0.084	234.06	0.003	8.37	0.004	11.15	0.013	36.26	0.018	50.22
3	0.083	154.18	0.004	7.44	0.005	9.29	0.015	18.59	0.011	20.46
4	0.082	114.24	0.006	8.37	0.015	20.92	0.016	22.32	0.016	22.32

3.3 Potentiodynamic polarization estimation

Figs. 3 and 4 provide the potentiodynamic polarization curves for GS and 304 SS in different conditions, respectively. Various corrosion parameters as corrosion potential (E_{corr}), anodic and cathodic Tafel slopes (β_a, β_c), the corrosion current density (I_{corr}), and the inhibition efficiency (*IE %*), are shown in Table 4. It can be seen that the inhibitor has a small effect on anodic Tafel consistent (β_a) estimates and a more important impact on cathodic Tafel steady (β_c) estimates, demonstrating that the inhibitor can alert the cathodic response instrument and may not have effect of anodic disintegration phase [22]. The change in values of cathodic Tafel slope (β_c) is propose that the response component of the hydrogen decrease is not the equivalent in the existence and absence of investigated inhibitor.

Table 5 illustrates clearly that the current density (I_{corr}) and CR values are decreased, as predicted in the existence of various concentrations of investigated inhibitor. The inhibiting activity is expanded with the concentration to arrive at the greatest estimation of 62.6 % and 59.4 % at 50 ppm for GS and

304 SS, respectively. The E_{corr} value moved in the negative direction by incorporating inhibitor. In addition, the negative corrosion potential change suggests that the compounds examined are consider cathodic inhibitor [23]. The abatement in the erosion current density and the expansion in the hindrance effectiveness might be credited to the physical adsorption of the investigated inhibitor on the GS or 304 SS surface. The results of the tests based on polarization curves revealed that in the presence of inhibitor, I_{corr} decreases dramatically at all concentrations studied. Tafel polarization technique affirmed the main WL results, giving some extra data. They are dictated by extrapolation of Tafel lines to the corrosion potentials.

Table 4. Corrosion parameters obtained from polarization curves for corroded GS in 1M H_2SO_4 with concentrations of investigated inhibitor (0-200 ppm) at RT.

Inhibitor concentrations in 1 M H_2SO_4 (ppm)	E_{corr} **mV**	I_{corr} **mA/cm^2**	β_a **mV/dec**	β_c **mV/dec**	***CR*** **mm/y**	θ	***IE*** **%**
0	-514	25.59	145	-139	299.3	--	--
50	-933	9.56	178	-160	111.8	0.626	62.6
100	-957	16.34	177	-52	191.1	0.362	36.2
150	-943	22.10	135	-117	258.4	0.136	13.6
200	-941	22.37	120	-114	261.6	0.125	12.5

Table 5. Corrosion parameters obtained from polarization curves for corroded 304 SS in 1M H_2SO_4 with concentrations of investigated inhibitor (0-200 ppm) at RT.

Inhibitor concentrations in 1 M H_2SO_4 (ppm)	E_{corr} **mV**	I_{corr} **mA/cm^2**	β_a **mV/dec**	β_c **mV/dec**	***CR*** **mm/y**	θ	***IE*** **%**
0	-282	1.59	200	-134	18.6	--	--
50	-305	0.64	249	-159	7.5	0.594	59.4
100	-304	0.74	183	-166	8.7	0.531	53.1
150	-319	0.83	174	-128	9.7	0.479	47.9
200	-334	0.95	212	-137	12.9	0.304	30.4

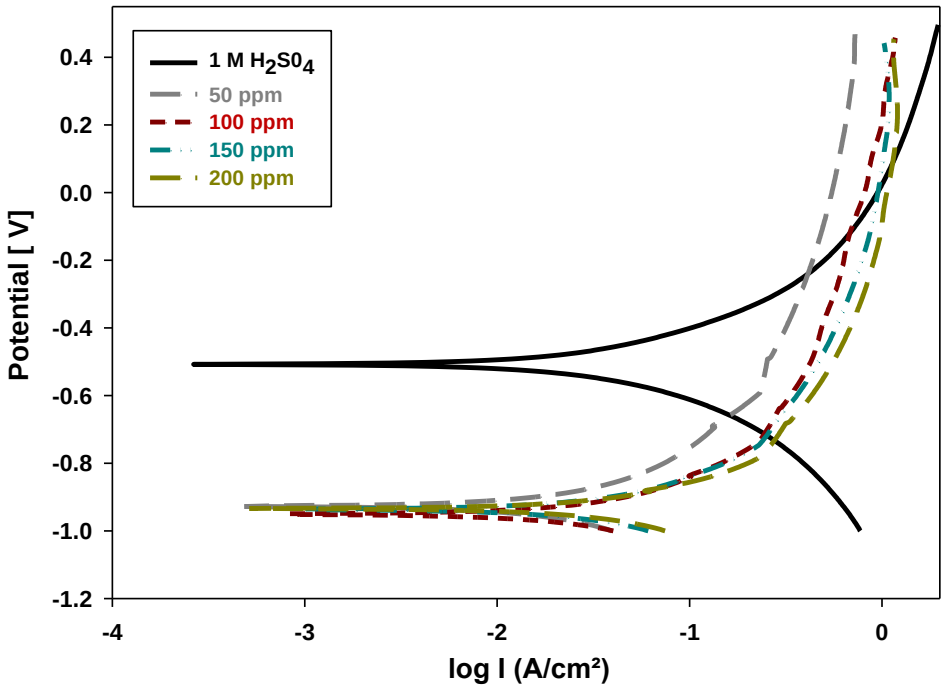

Figure 3. Potentiodynamic polarization curve for the corrosion of GS in 1M H_2SO_4 with concentrations of investigated inhibitor (0-200 ppm) at RT.

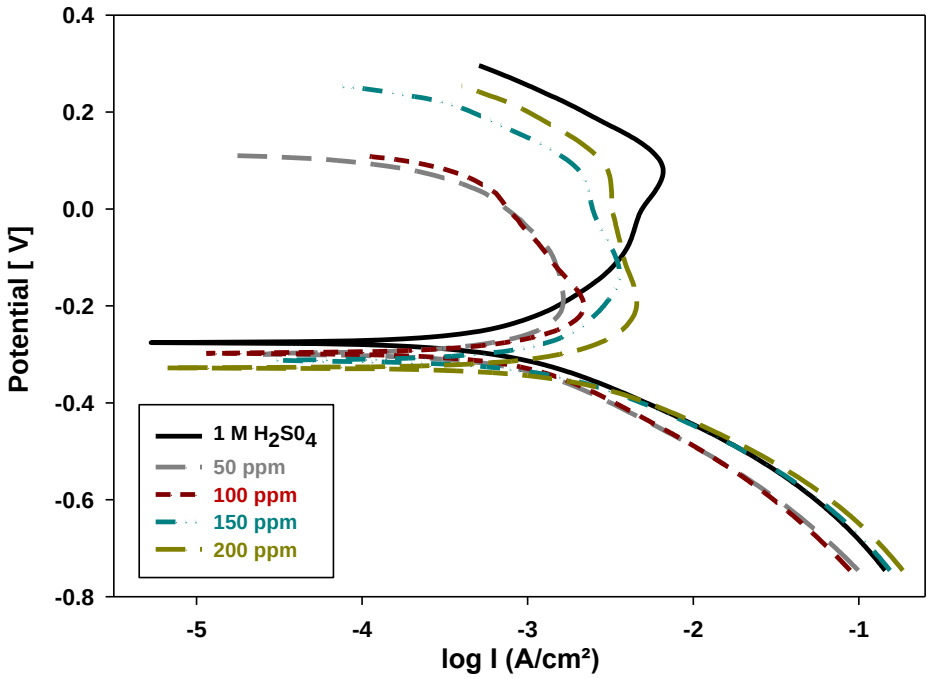

Figure 4. Potentiodynamic polarization curve for the corrosion of 304 SS in 1M H_2SO_4 with concentrations of investigated inhibitor (0-200 ppm) at RT.

3.4 Surface Morphology

The polished surfaces of GS and 304 SS immersed in 1M H_2SO_4 in the presence and absence of inhibitor were examined using SEM as provided in Fig. 5. The corroded surface was found with etched grain boundaries as provided in Fig. 5(a). The morphology indicates that the surface is strongly damaged in the absence of inhibitor (active corrosion). However, the micrographs in the presence of the inhibitor have a lower corrosion sites and pits over the surface as provided Figs. 5 (b and c) than without inhibitor. This could be related to the creation of an inhibitor adsorption layer on the specimen surface. Increasing the concentration from 50 to 200 ppm increasing CR as shown in Fig. 5. The compound with 50 ppm impair the GS. While increasing the concentration of inhibitor on 304 SS from 50 to 200 ppm increasing CR Fig. 6. The compound with 50 ppm improve the 304 SS. From these observations, it was found that the inhibitor had a good inhibition effect for the 304 SS matching with the WL estimation.

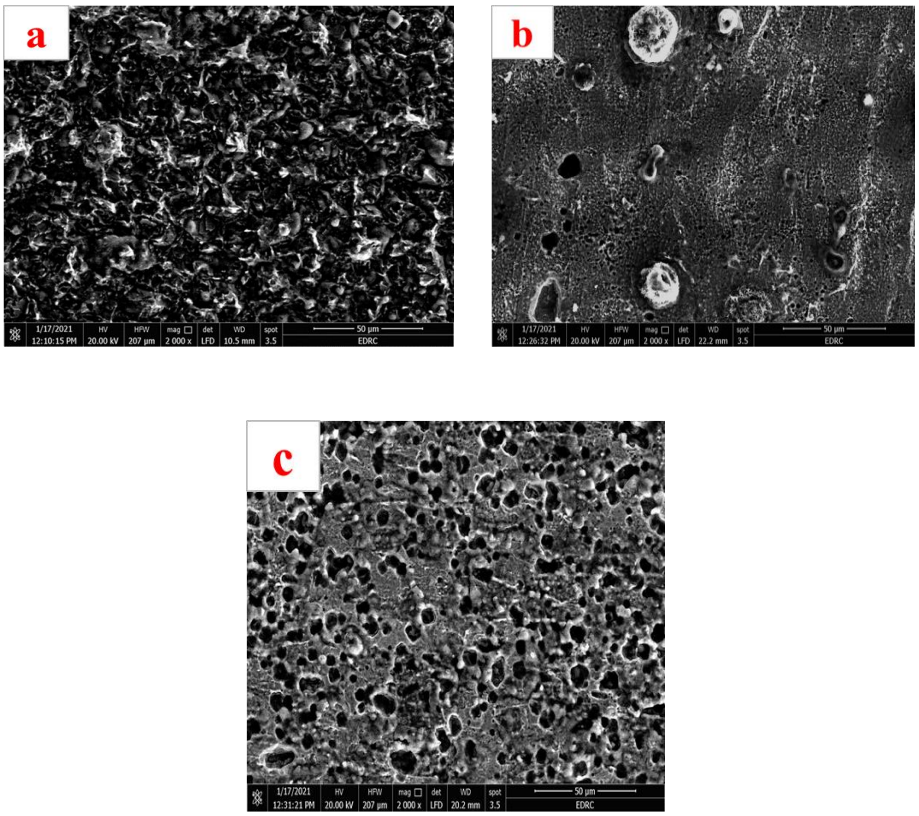

Figure 5. Scanning electron micrographs of GS after immersion in (a) 1M H_2SO_4 (b) 1M H_2SO_4+50 ppm (c) 1M H_2SO_4+200 ppm

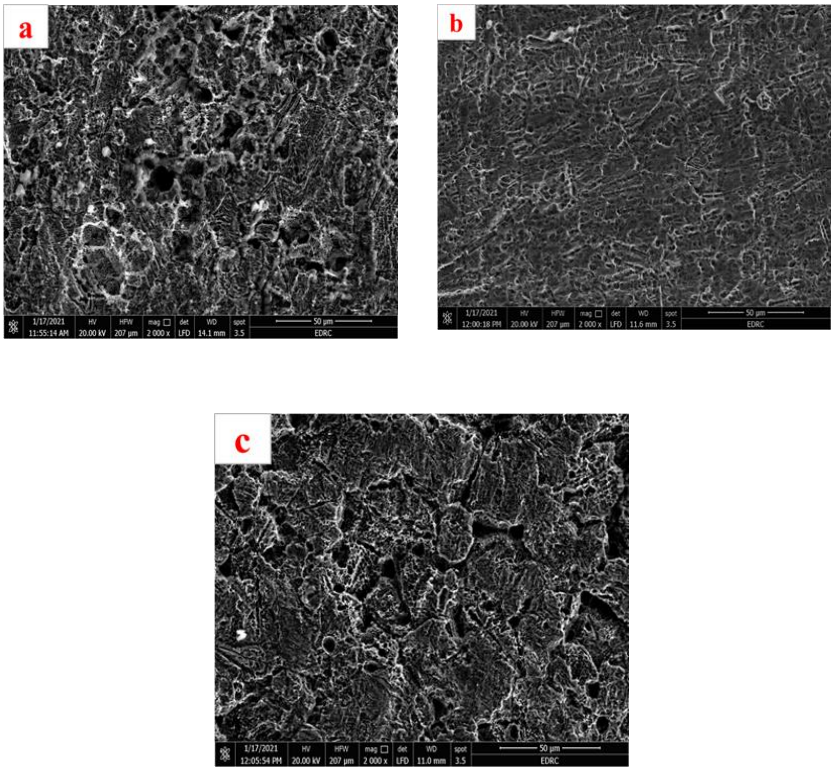

Figure 6. Scanning electron micrographs of 304 SS after immersion in (a) 1M H_2SO_4 (b) 1M H_2SO_4+50 ppm (c) 1M H_2SO_4+200 ppm

3.4 Theoretical studies of ligand

The prepared ligand CMBAH's 3D-optimized molecular structure has been adjusted, as illustrated in Fig. 7. The molecular parameters are the total energy, dipole moment, energy of the highest occupied molecular orbital (E_{HOMO}**)** and energy of the lowest unoccupied molecular orbital (E_{LUMO}), as given in Fig. 8, ΔE (the gap between the HOMO and LUMO energy levels, E_{gap}), chemical potential (pi), electrophilicity index (ω), absolute softness (σ), absolute hardness (η), and additional electronic charge (ΔN) were estimated [24] and tabulated in Table 6

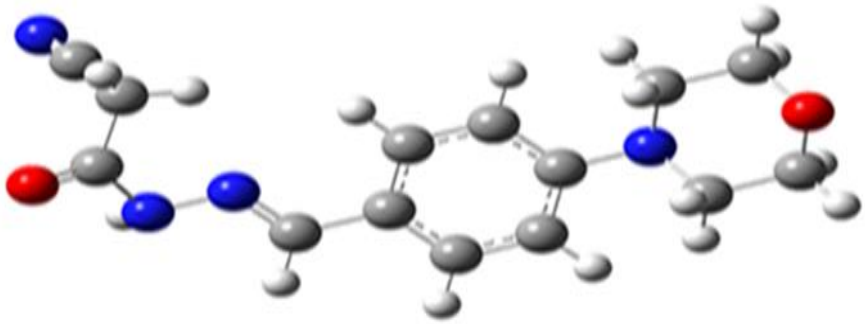

Figure 7. Modeling structure of ligand (CMBAH).

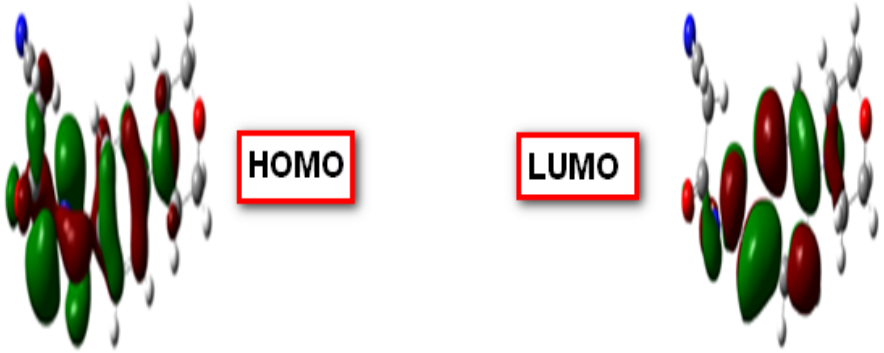

Figure 8. 3D plots frontier orbital energies using DFT method for CMBAH ligand.

Table 6. Theoretical and calculated quantum chemical parameters of molecular modeling of the ligand CMBAH.

Parameters	**CMBAH**
Total energy, (kcal / mol)	-5728.82
Dipole moment, (Debye)	6.3123
Chemical potential	-0.14257
E_{HOMO}	-0.2353
E_{LUMO}	-0.0785
ΔE	0.14256
η	0.07128
σ	14.02918
ΔN	2.0001
ω	0.14258

First, the reactivity index evaluates the energy stabilization when a system acquires an additional electronic charge (N) from the environment, according to the data. Electrophilicity index (ω) is positive, specific quantity, and the charge transfer direction is completely estimated by the electronic chemical potential (pi) of the molecule. Electrophile is a chemical species able to accept electrons from the environment and its energy must decrease upon accepting electronic charge. As a result, the electronic chemical potential must be negative as demonstrated in Table 6. Secondly, the high values of HOMO energy (E_{HOMO}) of the ligand under investigation HL reflects a great trend of that ligand to offering electrons to empty d orbitals of the metal ions that resulting in high interaction efficiency between the ligand and the metal ions. Finally, the LUMO - HOMO energy gap (ΔE) values of ΔE indicate that the ligand in the investigation has high inclination to bind with the metal ions. Another descriptor which

predict the ligand activity is molecular electrostatic potential (MEP) given in Fig. 9. MEP is also represented the active sites of love of nucleus and love of electron attack. In the obtained MEP, blue color (positive) regions are descriptions for the love electron sites but the red color (negative) regions are descriptions for love nucleus attack. All reactivity descriptors equations in this study summarized as reported elsewhere [25-27].

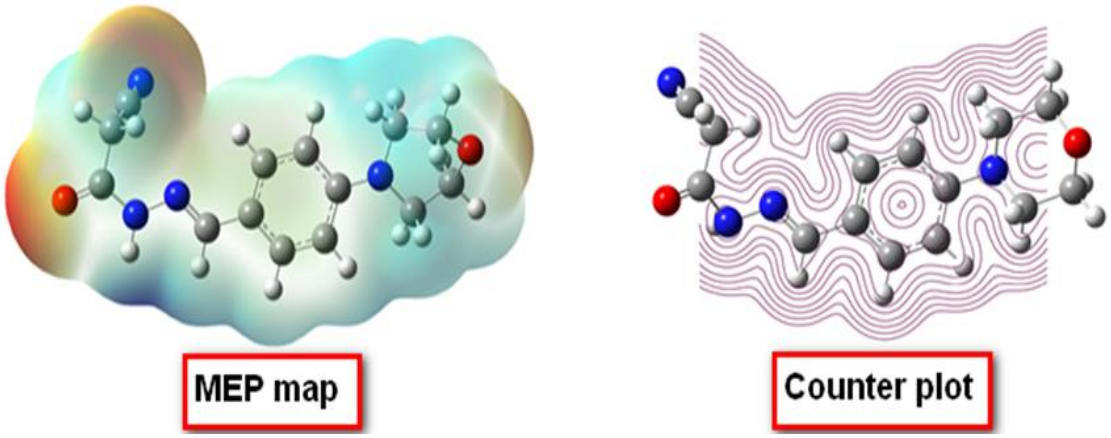

Figure 9. Schematic of MEP map and counter plots for CMBAH ligand

4. CONCLUSIONS

The corrosion behavior of GS and 304 SS in 1M H_2SO_4 solution using 2-cyano-N-(4-morpholinobenzyldine) acetohydrazide as a corrosion inhibition were investigated. It was demonstrated that the 2-cyano-N-(4-morpholinobenzyldine) acetohydrazide is effective inhibitors for the corrosion of 304 SS in 1M H_2SO_4 at 50 ppm concentration. Increasing the inhibitor concentration proportionally increases the inhibition efficiency. The compound inhibits corrosion by adsorption of this compound from acid solution follow Langmuir's adsorption isotherm for all concentrations. The surface micrographs of GS and 304 SS revealed the formation of a smooth and dense protective layer.

ACKNOWLEDGEMENT
The authors acknowledge Associate Prof. Yassar Reda (Higher Institute of Engineering and Technology Tanta) for English revision.

References

1. P. Shetty, *S. Afr. J. Chem*., 71 (2018) 46–50
2. B. Rapp, Mater. Today., 9(3) (2006) 6
3. H.H. Uhlig, R.W. Revie, Corrosion and Corrosion Control: An Introduction to Corrosion Science and Engineering, 3rd ed., John Wiley and Sons, New York, 11 (1991)

4. R.H. Taha, G.A. Gaber, L.Z. Mohamed, W.A. Ghanem, *Egypt. J. Chem*. 62 (Part 1) (2019) 367-381
5. S.K. Ahmed, W.B. Ali, N.A. Khadom, *J. Bio-Tribo-Corros*., 5 (2018) 15
6. S.I. Keny, A.G. Kumbhar, C. Thinaharan, G. Venkateswaran, *Corros. Sci.,* 50 (2008) 411-419
7. X. Zheng, M. Gong, Q. Li, L. Guo, *Sci. Rep*., 8 (2018) 9140
8. M.A. Quraishi, R. Sardar, D. Jamal, *Mater. Chem. Phys*., 71 (2001) 309–313
9. A. Quraishi, N. Saxena, D. Jamal, *Indian J. Chem. Technol*., 11 (2005) 220–224
10. S. Xia, Qiu M, L. Yu, L. Liu, H. Zhao, *Corros. Sci*., 50 (2008) 2021–2029
11. A.O. Yüce, B.D. Mert, G. Kardas, B. Yazıcı, *Corros. Sci*. 83 (2014) 310–316
12. G.A. Gaber, H.A. Aly, L.Z. Mohamed, *Int. J. Electrochem. Sci*., 15 (2020) 8229-8240
13. G.A. Gaber, L.Z. Mohamed, A. Jarvenp, A. Hamada, *Surf. Coat. Technol*., 423(15) (2021) 127618
14. L.Z. Mohamed, G. Hamdy, G.A. Gaber, *Int. J. Electrochem. Sci*., 16 (2021) 210515
15. A. Chacko, A.M.J. Newton, *Recent Pat Drug Deliv Formul*, 13(1) (2019) 46-61
16. V.S. Sastri, Green corrosion inhibitors: Theory and practice, Wiley, *Hoboken* (1998)
17. O. Olivares-Xometl, N.V. Likhanova, B. Gomez, J. Navarrete, M.E. Llanos-Serrano, E. Arce, J.M. Hallen, *Appl. Surf. Sci*., 252(6) (2006) 2894–2909
18. K. Al-Azawi, S. Al-Baghdadi, A. Mohamed, A. Al-Amiery, T.K. Abed, S.A. Mohammed, A.A. Kadhum, A.B. Mohamad, *Chem Cent J*, 10(1) (2016) 23
19. N.V. Likhanova, M.A. Veloz, H. Höpfl, D.I. Matías, V.E. Reyes-Cruz, O. Olivares, R. Martínez-Palou, *J Heterocycl Chem*, 44(1) (2007) 145–153
20. G. Chen, M. Zhang, I. Zhao, R. Zhou, Z. Meng, J. Zhang, *Chem. Cent. J*., 7 (2013) 83
21. L. Fomina, B. Porta, A. Acosta, S. Fomine, *J Phys Org Chem* 13 (2000) 705–712
22. H.B. Lokesh, P.F. Sanaulla, V.B. Bheema, *IOSR-JHSS,* 19(6) (2001) 9-20
23. A.S. Fouda, S.A. Abdel-Maksoud, A.E. Almetwally, *Chem. Sci.,* 4(4) (2015) 877-889
24. N.O. Obi-Egbedi, I.B. Obot, M.I. El-Khaiary, S.A. Umoren, E.E. Ebenso, *Int. J. Electrochem. Sci*. 6 (2011) 5649-5675
25. M. Ouakki, M. Galai, M. Rbaa, A.S. Abousalem, B. Lakhrissi, E.H. Rifi, M. Cherkaoui, *Heliyon*, 5 (2019) e02759
26. M. Rbaa, A.S. Abousalem, M. Galai, H. Lgaz, B. Lakhrissi, I. Warad, A. Zarrouk, *Arab. J. Sci. Eng.*, 46 (2021) 257–274
27. G. Mahalakshmi, V. Balachandran, *Spectrochim. Acta A Mol. Biomol. Spectrosc*., 135 (2015) 321–334